Shipley, T.H., Ogawa, Y., Blum, P., and Bahr, J.M. (Eds.), 1997
Proceedings of the Ocean Drilling Program, Scientific Results, Vol. 156

16. INTERPRETATION OF SITE 948 LOGGING-WHILE-DRILLING DATA: MINERALOGICAL INVERSION OF LOG DATA CONSTRAINED BY SAMPLE ANALYSES[1]

María José Jurado[2] and Belén Alonso[3]

ABSTRACT

This study is an original application of the log inversion methods on logging-while-drilling (LWD) measurements to clay mineral estimation in an unusual geologic setting: the Barbados accretionary prism. LWD was used for the first time by the Ocean Drilling Program during Leg 156 at Sites 947 (Hole 947A) and 948 (Hole 948A). At Site 948 the décollement zone was logged and cored. Hole 948C, located close to Hole 948A, was cored and logged with open-hole (conventional) logging tools. A model of the main mineralogical components identified at Hole 948C has been obtained from the inversion of LWD data from Hole 948A, using a methodology that is commonly applied on conventional logs. Density (RHOB), photoelectric factor (PEF), neutron porosity (TNPH), spectral natural gamma ray (SGR), and the spectral natural gamma ray Th/K ratio (Th/K) LWD data were used in the inversion. Hole 948C core sample analyses indicative of a clay-dominated "complex lithology" have been used to constrain the model and to test the quality of the results obtained. The inversion of log data provides a good approximation to the actual mineralogy, and the relative abundance of clay, and the main clay types. The deviation observed between the model and Hole 948C sample analyses results can be mostly explained by the presence of minerals not included in the inversion model. The porosity values calculated are close to shipboard "bulk water content" values. This model shows that the application of conventional log inversion techniques on a limited set of LWD data to quantitatively estimate trends in mineralogical changes can yield satisfactory results. The inversion model gives a good approach to the results obtained from X-ray diffraction for Hole 948C Units II and III sediments (420–580 mbsf) and constitutes the first inversion model for the composition of sediments obtained from the first LWD data of the Barbados accretionary prism. LWD data can be used to model mineralogical composition and porosity.

INTRODUCTION

Logging-while-drilling (LWD) data are the most complete record of the physical properties and the geology of Ocean Drilling Program (ODP) Leg 156 (northern Barbados Ridge accretionary prism) Sites 947 and 948 (Fig. 1). The northern Barbados Ridge accretionary prism is a convergent margin that is actively accreting oceanic pelagic/hemipelagic sediments (Moore et al., 1995), and it has been intensively studied by drilling during previous Deep Sea Drilling Project (DSDP) and ODP Legs 78 and 110, respectively (Mascle, Moore, et al., 1988; Moore et al., 1988). The most striking feature recorded by Leg 156 logs is the décollement, the boundary between the accretionary prism sediments and the underthrusting plate, that was successfully cored and logged at Site 948 (Shipley, Ogawa, Blum, et al., 1995). At Hole 948C hemipelagic clayey sediments from Unit II and Unit III (Shipley, Ogawa, Blum, et al., 1995) were cored between 420.8 and 592.72 mbsf in the décollement zone. Lower to middle Miocene claystone underlain by lower Miocene and upper Oligocene variegated claystone with muddy turbidites and redeposited chalk were recovered (Shipley, Ogawa, Blum, et al., 1995).

Clay mineralogical changes are relevant to the study of the décollement zone, as has been stated in previous studies in the area (Mascle, Moore, et al., 1988; Moore et al., 1988; Underwood and Deng, Chapter 1, this volume). The focus of this work has been to test the possibility of modeling the mineralogies recovered on cores at Hole 948C from LWD data, by using a conventional log inversion methodology as commonly applied on open-hole logs. Our results provide a mineralogy-porosity inversion model for the mineralogies encountered in the décollement zone.

The study has involved both sample analysis and log analysis. From Site 948 both core sample analyses (Hole 948C; Subunits IIA through IIF; Subunits IIIA and IIIB) and continuous LWD data (Hole 948A) have been used (Shipley, Ogawa, Blum, et al., 1995).

Inversion of mixed mineralogies is one of the most complex studies that can be undertaken from the analysis of logging data. Because log response accounts for both sediment composition and fluids, in addition to the estimation of mineral components, porosity has to be included as part of the system. The results obtained from the inversion of LWD data indicate that even in this case, which can be qualified as being of extreme complexity from the point of view of the log analysis, it is possible to obtain a good approximation to the actual composition of the sediments by inversion techniques. Our model could be constrained and calibrated to sample data. Our modeling results are to a great extent comparable and compatible with the laboratory analyses available. Besides this, the sources of misfit can also be constrained and explained by the presence of components that are not included in the model, given the limited set of log measurements and also by the log data quality.

LOGGING DATA

Schlumberger CDR (Compensated Dual Resistivity) and CDN (Compensated Density Neutron) (Schlumberger, 1992) tools were used to acquire LWD data at Sites 947 and 948 during Leg 156. The principles of these tools and further details on the acquisition are described in Shipboard Scientific Party (1995). The set of LWD measurements obtained includes density (RHOB), photoelectric factor (PEF), neutron porosity (TNPH), spectral natural gamma ray (SGR, CGR, Th, U, K), deep (ATR) and shallow resistivity (PSR), and the rate of penetration (ROPE). LWD results in overall good data quality

[1]Shipley, T.H., Ogawa, Y., Blum, P., and Bahr, J.M. (Eds.), 1997. *Proc. ODP, Sci. Results*,156: College Station, TX (Ocean Drilling Program).

[2]Geophysikalisches Institut, Universität Fridericiana Karlsruhe, Hertzstrasse 16, 76187 Karlsruhe, Germany. mjjurado@gpiwap4.physik.uni-karlsruhe.de

[3]Instituto de Ciencias del Mar, CSIC, Paseo Joan de Borbó s/n, 08039 Barcelona, Spain.

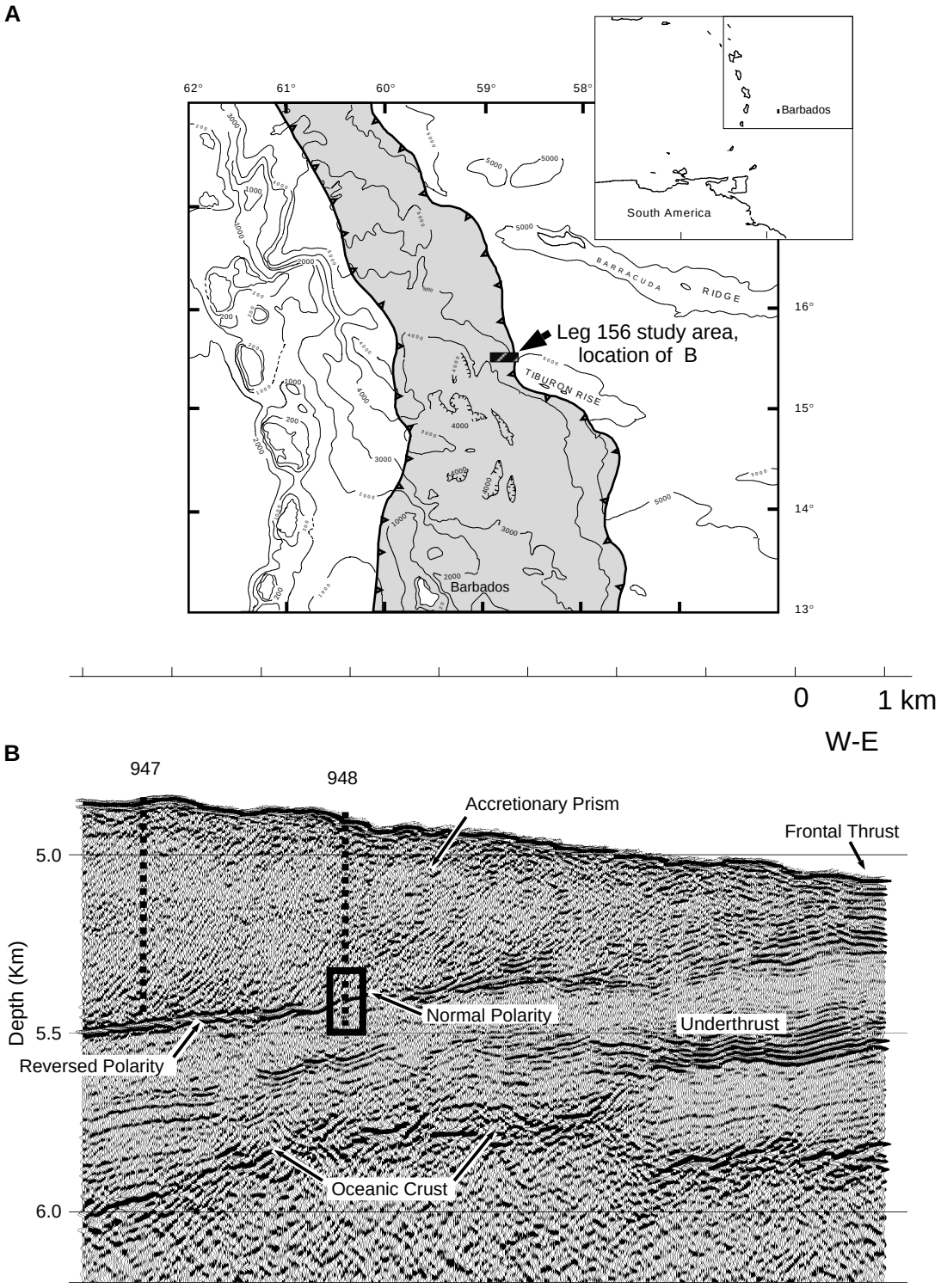

Figure 1. (**A**) Location map of Leg 156 and (**B**) seismic profile indicating the position of Sites 947 and 948 in the Northern Barbados accretionary prism. The boxed area (Site 948) corresponds to the interval analyzed in this study, the décollement zone.

Table 1. Sample analysis results from discrete Leg 156 Hole 948C samples.

Core, section	Depth (mbsf)	Lithologic subunit	$CaCO_3$ (wt%)	Sand (%)	Silt (%)	Clay (%)	Smectite (%)	Illite (%)	Kaolinite (%)	Chlorite (%)
156-948C-										
1H-1	.36	IA	12.7	19.88	27.70	52.42	—	—	—	—
1H-2	2.83	IA	24.0	15.38	26.08	58.54	—	—	—	—
2X-3	25.25	IIA	4.7	1.61	20.94	77.45	59	11	17	12
3X-5	437.11	IIA	5.8	.00	17.24	82.76	40	14	25	20
4X-1	441.15	IIA	3.6	.00	10.30	89.70	45	12	25	19
4X-6	447.72	IIB	9.5	.00	17.02	82.98	40	12	28	20
5X-3	453.27	IIB	4.0	.00	6.62	93.38	46	11	25	18
5X-5	456.02	IIB	7.1	.00	8.37	91.63	51	8	25	16
6X-1	460.50	IIB	4.6	.00	13.11	86.89	45	10	26	18
6X-5	465.63	IIC	4.9	.00	10.06	89.94	40	12	30	18
7X-1	469.14	IIC	6.1	.00	9.26	90.74	48	10	30	11
7X-5	475.24	IIC	4.5	.00	11.33	88.67	70	7	17	6
8X-1	479.44	IIC	3.9	.00	12.41	87.59	54	10	24	12
8X-6	486.99	IID	4.4	.00	17.29	82.71	58	9	21	11
9X-5	494.75	IID	3.7	.00	11.50	88.50	59	9	20	12
9X-CC	496.82	IID	3.7	1.16	17.51	81.33	61	9	19	11
10X-2	499.77	IIE	3.3	1.35	12.79	85.86	52	12	24	12
10X-2	500.85	IIE	4.7	1.39	15.55	83.06	40	8	41	11
11X-3	510.89	IIF	4.9	.00	10.37	89.63	35	8	39	17
11X-5	514.00	IIF	5.8	.00	40.15	59.85	38	14	34	14
12X-5	523.93	IIIB	3.3	.00	49.97	50.03	35	16	34	16
12X-5	524.53	IIIB	3.7	.00	17.15	82.85	67	9	17	7
13X-3	530.61	IIIB	31.0	.87	32.22	66.92	29	10	39	22
13X-3	530.69	IIIB	30.0	23.56	60.97	15.47	31	21	28	20
14X-CC	545.33	IIIB	4.8	.00	33.26	66.74	42	15	30	13
14X-CC	545.41	IIIB	5.1	.00	36.18	63.82	—	—	—	—
15X-1	546.54	IIIB	35.1	.00	35.64	64.36	29	9	43	18
15X-3	548.88	IIIB	6.7	.00	21.37	78.63	35	16	36	12
16X-6	562.32	IIIB	4.3	.00	7.87	92.13	42	16	28	14
16X-6	562.47	IIIB	4.6	.00	35.31	64.69	33	15	36	16
17X-4	570.04	IIIB	33.6	.00	66.30	33.70	35	10	34	21
17X-7	573.14	IIIB	34.0	.00	14.42	85.58	22	8	53	16
17X-76	573.27	IIIB	35.2	4.10	72.33	23.57	35	10	40	16
18X-3	576.34	IIIB	32.0	.00	52.76	47.24	31	15	40	15
18X-3	576.69	IIIB	3.8	.00	7.38	92.62	21	15	40	24
18X-3	576.83	IIIB	9.0	.00	45.59	54.41	34	13	32	21
19X-4	587.31	IIIB	51.9	.00	54.03	45.97	—	—	—	—
19X-CC	592.37	IIIB	29.3	.00	20.70	79.30	—	—	—	—

Note: — = no data, wt% = weight percent.

according to data quality control report (LDEO, unpubl. data), performed at Lamont-Doherty Earth Observatory by the Borehole Research Group. Nevertheless, the rate of penetration log (ROPE) indicates that logging speed was too high for accurate natural gamma ray spectral data acquisition and resulted in localized bad readings and low values. LWD data were depth shifted to the seafloor –4950 m for Hole 948A.

Open-hole (conventional) logs were also acquired at Hole 948C, but because of tool sticking and the overall bad hole conditions encountered, the quality of the wireline logs is poor. Hole 948C spectral natural gamma-ray (NGT) data were corrected for borehole size and drilling fluid and acoustic data (sonic log) for cycle skipping. Irregular borehole affected most measurements, especially the density log. The open-hole logs are of less quality than the LWD measurements and have not been included in this study.

METHODOLOGY

The approach used for mineralogy inversion from borehole log data is based on the principle that the log responses may be related to the sum of proportions of the mineralogical components considered, each multiplied by the appropriate response coefficients in a system of linear equations that can be solved simultaneously. The equations for each log take the form

$$c_1v_1 + c_2v_2 + \ldots\ldots c_nv_n = L,$$

where n is the number of components, v_i the proportion of component i, c_i the log response of component i, and L the log response. Each log provides a single equation. This matrix formulation is a linear model introduced by Savre (1963) and further developed by Burke et al. (1967). More extensive details on this methodology are given by Doveton (1994).

This approach provides generally satisfactory results if the main components are known, the appropriate set of logs is available and adequate coefficients are chosen. In our case, the main mineralogical components (n) are known from Hole 948C core sample analyses, the set of LWD "lithology" logs available (L) is limited, and both the coefficients (c) and the proportions of each component (v) are the main unknowns addressed and tested. The coefficients were initially chosen from published standard values or ranges for the components considered. The coefficients have been adjusted within the standard ranges, in accordance with the modeling results obtained, through successive iterations.

A large number of lithological and/or mineralogical components requires a large number of logs. Pore-fluids have been included as one more component in so far as they contribute to the log response. When the number of logs is less than the number of components by one, the equations satisfy the unknowns because of material balance the proportions of the components sum to one. A unique solution is obtained from the appropriate matrix algorithm by a conventional simultaneous equation technique. Further discussion on the theoretical aspects of this approach is given in Doveton and Cable (1979).

The full set of Hole 948A LWD measurements has been analyzed although only density (RHOB), photoelectric factor (PEF), neutron porosity (TNPH), spectral natural gamma ray (SGR), and the spectral natural gamma-ray Th/K ratio (Th/K) data were quantitatively used in the final inversion.

The inversion of mineral components from log data, including clay mineralogies, required good constraints on the mineralogical components. The constraints for the model come from 3 sets of core analysis results: the results obtained on discrete samples analyzed for texture and composition (Table 1), clay mineralogy results (for <1-

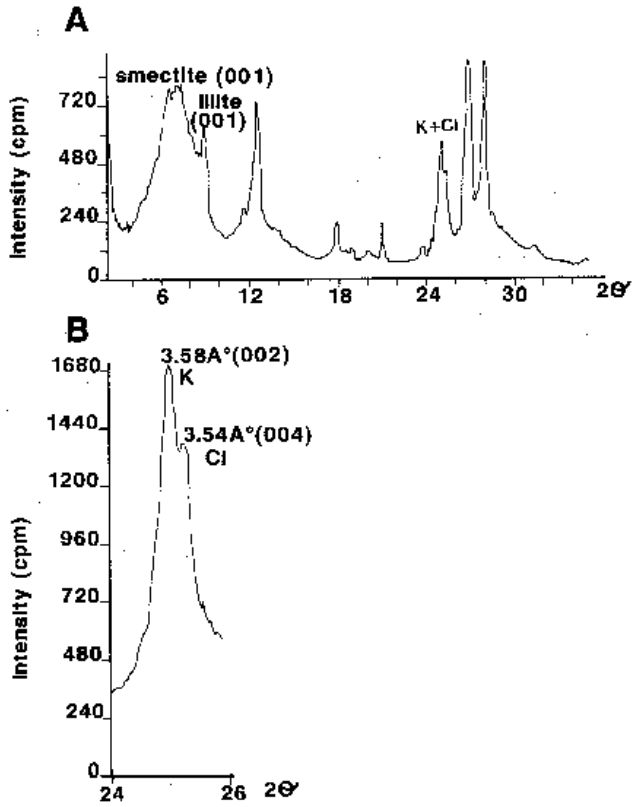

Figure 2. X-ray diffractograms: **A.** Positions and intensities of basal reflections for smectite, illite, and kaolinite. **B.** Kaolinite (3.58°) and chlorite (3.54°) reflections in the slow scan.

The inversion of mineral components from log data, including clay mineralogies, required good constraints on the mineralogical components. The constraints for the model come from 3 sets of core analysis results: the results obtained on discrete samples analyzed for texture and composition (Table 1), clay mineralogy results (for <1-µm fraction) obtained by Underwood and Deng (Chapter 1, this volume), and shipboard analyses (Shipley, Ogawa, Blum, et al., 1995).

Thirty-eight samples were analyzed for carbonate content, texture, sand fraction composition, and clay mineralogy in order to characterize sediment types, and relative abundance. Carbonate contents were determined using a Bernard calcimeter (Vatan, 1967) and are expressed as weight percent (wt%) $CaCO_3$ (assuming all carbonate as pure calcite). Sediment texture was determined by settling-tube techniques for the coarse-grained fraction (>50 µm), and Sedigraph 5000D techniques for the silt and clay fractions (<50 µm) (Giro and Maldonado, 1985). Sand fraction (>63 µm) composition was examined with a binocular microscope to estimate abundance of different components, counting about 250–300 grains per sample.

The clay mineralogy was determined in the fraction <2 µm. This fraction was collected by decantation, and orientated aggregates were made on glass slides. The X-ray diffractograms were made on an untreated sample, a glycolate sample, and a sample heated for 2 hr at 550° C. X-ray diffractograms were obtained with a Siemens d-500 X-ray diffractometer. Peaks were scanned from 2θ of 4° to 50°, with a step-scan range of 1.2θ–2.0θ, an angular increment of 0.05/2θ, and counting rate of 3 s/step. Diffractograms were visually interpreted with the aid of a computerized search-and-match routine based on the "Joint Committee on Powder Diffraction Standards" fields (International Centre for Diffraction Data, 1994).

The clay minerals identified by their characteristic basal-reflection maxima include smectite (001), illite (001), kaolinite (002), and chlorite (004) (Fig. 2). The two latter minerals are differentiated by the relative intensities; at 3.58° for kaolinite and 3.54° for chlorite reflections in the slow scan situated these peaks are between 24° and 26° (Biscaye, 1964). The relative proportions of clay minerals were estimated following the methodology proposed by Rius et al. (1989), a simple standardless method to directly determine calibration constants using only diffracted intensities and calculated phase-absorption coefficients by a least-squares procedure. This quantitative clay analysis has been successfully used to analyze marine sediments (Palanques et al., 1990; Alonso et al., 1996).

According to the sample analyses results and shipboard mineralogy results (Shipley, Ogawa, Blum, et al., 1995), the components to be considered were quartz, plagioclase, carbonate, smectite, illite, chlorite, and kaolinite, which can be regarded as the components of a "complex lithology".

CORE LOG INTEGRATION: RESULTS OF SAMPLE ANALYSES AND CORRELATION WITH LOG RESPONSE

Sample analyses results for mineral composition, texture and clay types are shown in Table 1. The correspondence between these results and borehole log data was examined by means of a correlation matrix (Table 2).

The sample analyses results correspond to core samples from Units I, II, and III as defined in Shipley, Ogawa, Blum, et al. (1995) and are listed in Table 1 and shown graphically in Figures 3 and 4.

Composition and Texture

The particle-size distributions of selected samples from beneath and above the décollement, the depth interval included in the model, were determined for 36 samples ranging from late Miocene to late Oligocene in age. Composition and texture of samples from Unit II correspond predominantly to fine-grained size: terrigenous clay (usually >90% clay) and terrigenous silty clay (77%–90% clay). Carbonate content is low (3.7%–13%) and its vertical distribution is uniform. Higher carbonate contents are found within Subunit IIB (Shipley, Ogawa, Blum, et al., 1995).

Sharp sediment texture changes are recognized within Unit III, and frequent fluctuations in composition and sediment texture occur within Subunit IIIB. Sediments range in composition and texture from most abundant terrigenous mud (30%–50% clay; 17%–49% silt) to terrigenous clay (>85% clay) of low carbonate content (3%), less frequent biogenic mud (67% clay, 32% silt), and biogenic sandy silt (60%–72% silt; 23% sand) with a relatively high carbonate content (30%–35%). Carbonate content within Subunit IIIB is locally high, and vertical distribution is irregular, showing considerable fluctuations ranging from 4% to 51%.

Two samples from Unit I, the uppermost cored interval (156-948C-1H-01, 0.36 mbsf and 156-948C-1H–02, 2.83 mbsf), correspond to silty clay (<58% of clay) containing major proportions of (biogenic) sands (15%–20%). These sediments are characterized by a high carbonate content (24%) and the abundance of biogenic components (90%). This depth interval and these results have not been included in the inversion model.

Clay Mineralogy

Clay is the most abundant textural component identified in the samples throughout the section (Table 1). Mineralogy analyses on the clay-size fraction of the samples yield the relative content (%) of the four clay minerals that have been identified: smectite, illite, kaolinite and chlorite.

The smectite content ranges from 38% to 72%, the average value for Unit II being 53%. Maximum values correspond to clay sediment

Table 2. Correlation matrix of log data and textural-mineral components from Table 1.

	SGR	CGR	Th/K	RHOB	PEF	TNPH	$CaCO_3$	Sand	Silt	Clay	Smectite	Illite	Kaolinite	Chlorite
SGR	1	.6366	.3697	.6202	.4953	–.3346	.4466	.2383	.5731	–.5550	–.5195	.5662	.4595	.1722
CGR	.6366	1	.2292	.3910	.4290–	.4740	.1384	.1463	.4100	–.3923	–.1172	.3242	.1600	–.1874
Th/K	.3697	.2292	1	–.1523	–.2582	–.2439	.0459	–.0326	.2296	–.1918	–.2125	.0745	.4174	–.2199
RHOB	.6202	.3910	–.1523	1	.8941	–.0062	.4234	.1954	.3849	–.3847	–.2708	.2797	.1665	.2312
PEF	.4953	.4290	–.2582	.8941	1	.0747	.2411	.0915	.2077–	.2035	–.2829	.2975	.1502	.2662
TNPH	–.3346	–.4740	–.2439	–.0062	.0747	1	–.3311	–.0836	–.4725	.4257	.2533	–.1626	–.2803	–.1125
$CaCO_3$	.4466	.1384	.0459	.4234	.2411	—.3311	1	.4142	.6688	–.6738	–.5385	.0965	.4630	.5523
Sand	.2383	.1463	–.0826	.1954	.0915	–.0836	.4142	1	.4620	–.6354	–.2186	.5449	–.0197	.2142
Silt	.5731	.4100	.2296	.3849	.2077	–.4725	.6688	.4620	1	–.9779	–.5268	.4841	.3961	.3757
Clay	–.5550	–.3923	–.1918	–.3847	–.2035	.4257	–.6738	–.6354	–.9779	1	.5086	–.5541	–.3388	–.3728
Smectite	–.5195	–.1172	–.2125	–.2708	–.2829	.2533	–.5385	–.2186	–.5268	.5086	1	.5061	–.8793	–.7573
Illite	.5662	.3242	.0745	.2797	.2975	–.1626	.0965	.5449	.4841	–.5541	–.5061	1	.1758	.318
Kaolinite	.4595	.1600	.4174	.1665	.1502	–.2803	.4630	–.0197	.3961	–.3388	–.8793	.1758	1	.4638
Chlorite	.1722	–.1874	–.2199	.2312	.2662	–.1125	.5523	.2142	.3757	–.3728	–.7573	.318	.4638	1

Note: SGR = natural radioactivity, CGR = computed natural radioactivity, Th/K = natural spectral thorium/uranium ratio, RHOB = density, PEF = photoelectric factor, TNPH = neutron porosity.

Kaolinite values range from 13% to 41% within Unit II. The highest values correspond to the base of Unit II (34%–41%). Kaolinite content ranges from 17% to 54% within Unit III.

High kaolinite content (~40%) corresponds to moderate $CaCo_3$ content (4.7%, 4.9%) within Unit II, but high $CaCO_3$ (>30%) locally within Unit III.

Chlorite content ranges from 6% to 20% within Unit II. Vertical distribution is regular and the average value is 14%. Within Unit III values are relatively higher; the average value is 18% and the distribution is even more variable.

Correlation of Sediment Composition with Log Response

A qualitative analysis of the some of the log curves displayed in Figure 3 reveals the main geological features of the décollement zone. Moderate variations in gamma-ray values, and locally in density and photoelectric factor values, correlate with slight changes in sediment composition within Unit II. These were the basis for identifying six lithostratigraphic subunits that are recognizable on the LWD data (Fig.3; Shipley, Ogawa, Blum, et al., 1995). The most striking change in all log values occurs at 513 mbsf and corresponds to the boundary between Unit II and Unit III, the boundary between the accretionary prism sediments and the underthrust sediments. Another sharp break in compositional changes can be located at about 520 mbsf, where a Th/K spike is remarkable. A deflection in the log values within Unit III at 525 mbsf, recognizable in the SGR, RHOB, TNPH, PEF, and Th/K logs corresponds to the boundary between Subunit IIIA and Subunit IIIB. Subunit IIIA is dominated by variegated claystones and Subunit IIIB by calcareous turbidites, silty terrigenous turbidites and hemipelagic claystones. Composition and textural changes recognized within Subunit IIIB have a good correspondence with changing log values and a "spiky" shape recognizable on natural-gamma ray neutron and photoelectric factor logs (Fig. 3). Carbonate-rich intervals result in higher density values and lower natural radioactivity (low K content) than the sediments within which the interbeddings occur. The vertical resolution obtained with the CDN tool for density log (15–5 cm) is within the range required for the identification of these levels within Subunit IIIB.

In addition to these main features, more subtle compositional trends that could be recorded by the LWD measurements have been analyzed by combining the log data and the results obtained from sample analyses.

The results of sample analyses from the décollement zone were quantitatively compared with log measurements by means of a correlation matrix (Table 1). Even considering the scattering of the samples and an unavoidable possible depth misfit between the samples and the log measurements, this analysis is useful to constrain how sensitive the different log measurements are to the corresponding compositional changes and also to choose appropriate logs for the inversion.

The correlation coefficients calculated show interesting features (Table 2). SGR displays a better correlation than CGR (computed natural radioactivity without uranium spectra) to all the mineral components. This feature is surprising in the case of the correlation between the gamma ray logs (SGR or CGR) and the clay minerals (except for chlorite) and suggests that the different clay minerals are characterized by different uranium contents. Although CGR is generally preferred for clay typing, we selected SGR for inclusion in the inversion model because of its observed correlation in this setting. Positive correlations were also observed between RHOB and SGR (also CGR) and between RHOB and PEF.

Correlations between mineral components include a positive correlation between carbonate and silt (0.66) and negative correlations between carbonate and total clay (–0.67) and smectite (–0.53). For clay minerals, smectite shows a negative correlation with kaolinite (–0.87) and chlorite (–0.75).

MINERALOGY INVERSION FROM LOG DATA

On the basis of the results of shipboard and shore-based core sample analyses, the main mineral components represented in the décollement zone are well constrained. Smectite, illite, chlorite, kaolinite, carbonate, quartz, and plagioclase are the main components of the sediments at Site 948 between 420.8 and 592.7 mbsf (Units II and III).

Textural analyses indicate that the clay fraction is the main textural component (>70%). Carbonate content is on average far below 10% for most of the section (Fisher and Underwood, 1995; Shipley, Ogawa, Blum, et al., 1995, p. 108; Table 1, this paper). Carbonate-rich samples (>20%) correspond to Subunits IA, IIA, IIB, and IIIB. The most carbonate-rich interval corresponds to the upper Oligocene calcareous turbidites within Subunit IIIB correspond. Quartz and plagioclase are also represented, although plagioclase content is very low within Unit III (Shipley, Ogawa, Blum, et al., 1995, p. 108).

The limited set of logs available and the number of mineral components, and thus of unknowns to be modeled in the inversion of log data, yields an underdetermined system. The importance of the different mineral components was evaluated in order to simplify the problem and reduce the number of unknowns. The clay types identified in sample analyses produce radically different log responses. The log response can vary strongly depending on Fe-Mg-Al, Ca-Na, and K contents of the clays, and these can vary for a same clay type. The amount of compositional water in clays also has a crucial influence on log values. Standard log density (RHOB) values for the clay minerals considered (Tables 1, 2) can range from 2.12 to 2.77 g/cm^3 and photoelectric effect (PEF) from 1.83 to 6.30. Thus, the variability of log values between chlorite and smectite is greater than, for example, between smectite and calcite, or quartz and plagioclase. Natural radioactivity properties and Th, K and U contents are also different

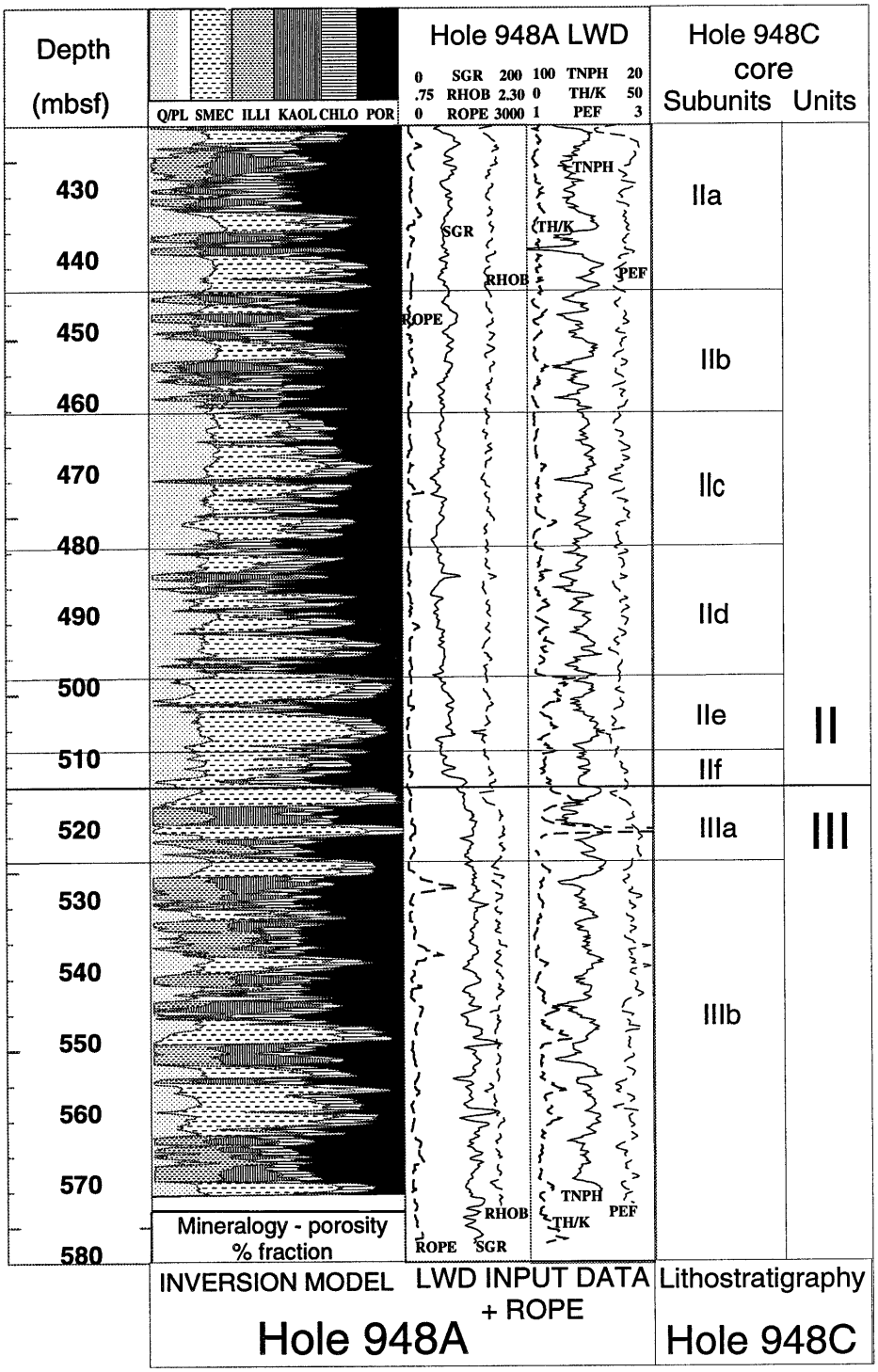

Figure 3. Site 948 décollement zone, between 420.8 and 580 mbsf. Mineralogy-porosity inversion performed on Hole 948A LWD data: quartz and plagioclase (Q/Pl), smectite (SMEC), illite (ILLI), kaolinite (KAOL), chlorite (CHLO), and porosity (POR). Computed percentages of mineral components and porosity were obtained applying Table 3 coefficients. To the right of the mineralogy inversion results are the logging data on which the mineralogy-porosity inversion was performed: density (RHOB), natural radioactivity (SGR), natural spectral thorium-uranium ratio (Th/K), neutron porosity (TNPH), and photoelectric factor (PEF) logs, and the rate of penetration (ROPE) log for quality control of LWD data.

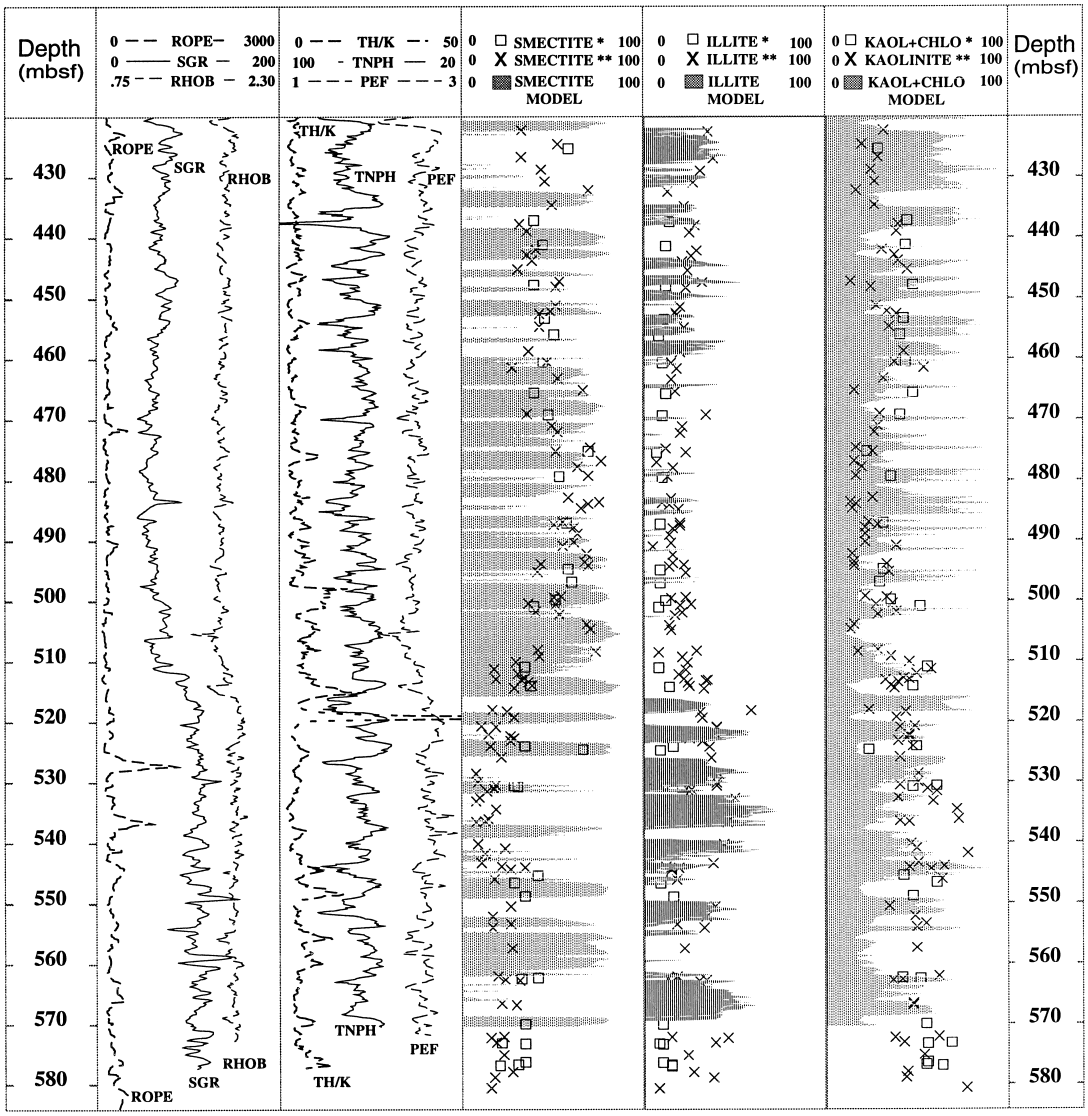

Figure 4. Core-log mineralogy integration for Site 948 décollement zone: correlation between core-derived and log-derived clay mineralogies. The first set of traces contains the LWD logs. In the following columns the percentage of smectite, illite, and kaolinite + chlorite to total clay are represented. The shading corresponds in each case to log-modeled values. Open squares correspond to Table 1 sample analysis values; crosses correspond to values obtained by Underwood and Deng (Chapter 1, this volume) for the clay size fraction <1 µm.

for these clay types; radioactivity values can vary significantly even for a same clay type (Schlumberger, 1982; Serra, 1986). Because of this variability the different clay minerals have been included as different components in the model.

Quartz and plagioclase produce relatively similar log responses and are therefore combined in a single component (Q + plag). Carbonate content is generally low throughout the décollement zone although it is locally high (>20%) within Subunit IIIB (carbonate-rich turbidites, Table 1). Being the least abundant component and given the limitation of a reduced set of LWD measurements (equations), it has been excluded from the inversion model and consequently the system is determined (6 unknowns, 5 logs, 6 equations).

The bulk spectral gamma ray (SGR), Th/K ratio log obtained from the spectral Th (ppm) and K (%) logs, density (RHOB), photoelectric factor (PEF), and neutron porosity (TNPH) were used in the calculations once resistivity measurements were discarded because of the complex response of resistivity measurements to porosity, fluids, and cation exchange capacity (CEC) that is subject to study at present (Henry, Chapter 10, this volume). However, deep resistivity measurements (ATR) show good correlations with clay mineralogies

The interest in the use of the spectral data is obvious, since natural gamma-ray spectral data are commonly used for clay-typing. The Th/K ratio is a function of the mineralogical composition of shales (Schlumberger, 1982). Thorium content reflects the aluminum content of the clay. Of the clay minerals identified, only illite contains K.

The coefficients used to perform the inversion are shown in Table 3 and correspond to standard log values that can be found in Serra (1986) for density (RHOB), photoelectric effect (PEF), bulk natural radioactivity (SGR), and neutron porosity (TNPH), and in the ranges given in Schlumberger (1982, 1985) for the Th/K value. For the Q + plagioclase component an averaged (quartz-plagioclase) standard log value has been used. RHOB and TNPH values for porosity correspond to low salinity and freshwater respectively.

The goodness of the inversion model is evaluated in relationship to the mineral composition obtained from the core samples, as judged from a graphical comparison (Fig. 4) and also by comparison be-

Table 3. Coefficients used for the mineralogy inversion of log data.

Log component	RHOB (g/cm^3)	SGR (API)	Th/K	TNPH (p.u.)	PEF (barn/el)
Q/PL	2.65	5.0	3.0	4.0	2.0
SMEC	2.12	180.0	12.0	44.0	2.04
ILLI	2.53	280.0	3.50	30.0	3.45
KAOL	2.42	100.0	14.0	37.0	1.83
CHLO	2.77	215.0	16.0	52.0	6.3
POR	1.09	0.0	0.0	100.0	0.8

Notes: Quartz and plagioclase (Q/PL), smectite (SMEC), illite (ILLI), kaolinite (KAOL), chlorite (CHLO), and porosity (POR) are the components. Density (RHOB), natural radioactivity (SGR), natural spectral thorium/uranium ratio (Th/K), neutron porosity (TNPH) and photoelectric factor (PEF) are the logs. Barn/el = barns/electron, p.u. = neutron porosity units.

tween the average values obtained from sample analysis and from the inversion of the log data (Table 4).

Even though the inversion model reproduces the trends and relative abundances of the components considered, some sources or error are known beforehand. Most of these problems are related specifically to log acquisition during Leg 156 and could be reduced in future LWD acquisition. Logging speeds were far above those recommended for natural gamma ray spectral data acquisition and this affects the accuracy of the measurements.

Some of the logs used show strong correlation (Table 2). More independent log measurements would be desirable. For example, PEF measurement is strongly correlated (.8941) with RHOB and probably does not add significant independent information to better discriminate between mineralogical components.

The results of bulk mineralogy-porosity inversion are displayed in Figure 3. In Figure 4, the results obtained for the different clays content are compared with Hole 948C (420.8–592.72 mbsf) core sample analysis results from Table 1, and from Underwood and Deng (Chapter 1, this volume). In order to compare with core sample analysis results on clay mineralogy, the scores obtained from the bulk mineralogy-porosity calculation were converted to percentage of total clay. Kaolinite + chlorite, calculated separately, are plotted together as KAOL + CHLO in Figure 4.

DISCUSSION OF THE INVERSION MODEL

The results obtained (Figs. 3, 4) indicate a good agreement between sample analysis results and results obtained from mineralogy modeling from a limited set of log data.

The core sample analysis results of Underwood and Deng (Chapter 1, this volume) and those from Table 1 are taken as the "true" reference to which the model is compared (Fig. 4; Table 4). We recognize that there may be inaccuracies as a result of both limitations of sample analysis methods and discrepancies between core-measured and log-measured depths.

The solution obtained from the inversion of log data is not perfect (Fig. 4; Table 4), but it yields a good approximation to the measured core sample mineralogy when using standard log values, log values within the standard ranges (Schlumberger 1985; Serra 1986) or averaged standard log values (Q + plagioclase) for the minerals considered in the system (Table 2). Different choices for the matrix coefficients, within the standard values ranges, would yield slightly different mineral-porosity proportions. Our results are a first attempt but this methodology needs further testing and refinement that will be gained with the study of other cases in the future.

Some uncertainty arises also regarding the accuracy of the LWD measurements that might have been affected by fast logging speeds. The magnitude of this effect for the different logs will be better constrained by the acquisition of new LWD data. Nevertheless, the results obtained suggest that most log measurements were not dramatically affected.

On the basis of the procedure followed in the inversion, a major cause for inaccuracy beforehand could be the presence of minerals not accounted for in the system. Carbonate is the most important of these according to sample analyses (Tables 1, 4), but others that were also identified shipboard (e.g., phillipsite, rich in K and H_2O) could attain significant concentrations locally. The "Q + plagioclase" component is assigned a single averaged value for the whole interval within the model, although it is known from shipboard analyses (Shipley, Ogawa, Blum, et al., 1995) that plagioclase content is very low within Unit III.

The Q + plagioclase log-calculated average value (20%) is slightly lower than that obtained from shipboard analyses (Fisher and Underwood, 1995; Shipley, Ogawa, Blum, et al., 1995, p. 111), but the major increases and decreases with depth that can be observed in Figure 3 are in good agreement.

The density coefficient used for Q + plagioclase density is that of quartz. If anorthite (log density = 2.76 g/cm^3) were the main constituent of plagioclase, then the density coefficient used in the inversion would be too low. For albite, the log density value is very close to that of quartz and no error should be expected.

In general, for clay mineralogies there is a good agreement (Fig. 4) between log calculated values (shading) and sample analysis results (crosses and triangles). Table 4 shows the averaged values obtained in each case. The model gives a good approach to smectite and illite contents. The approach also works well for kaolinite + chlorite but a considerable deviation is observed if those minerals are considered separately. Probably the inversion fails to differentiate the two minerals. There is a good correlation between the interval where greater differences exist (Subunit IIIB) and the occurrence of high $CaCO_3$ in core samples, suggesting that because the carbonate content is not accounted for in the model, the calculations are affected.

The porosity values calculated (31.7% average value for the interval 420 to 570.5 mbsf) are lower than those obtained from shipboard core samples (56.5% average value; Shipley, Ogawa, Blum, et al., 1995) but these may include compositional water as well as interstitial porosity. Recent studies by Henry (Chapter 10, this volume) also suggest that the physical properties porosities could be overestimated. Our calculated values compare fairly well with the "bulk water content" (30.3%) obtained shipboard (Shipley, Ogawa, Blum, et al., 1995).

CONCLUSIONS

LWD data can be used to model mineralogical composition and porosity. The mineralogy model obtained from the inversion of Site 948 LWD data, which is well constrained by sample analyses, confirms that logging data can give a good approximation of relative mineral content.

The interpretation of Site 948 LWD data and the results obtained from the inversion of log data reveal that LWD can be a valuable tool for the interpretation of uncored sections applying the inversion methodology tested here.

The best log-mineralogy inversion results are obtained for total clay, smectite and illite. The values obtained for porosity are reasonable considering that the "compositional water" of water-rich clay minerals would not be included in the porosity calculated by the inversion model.

ACKNOWLEDGMENTS

Logging-while-drilling data acquisition was funded by JOI/USSAC and the U.S. National Science Foundation. This research was supported by two Spanish CICYT grants (AMB94-1410-E, AMB95-0196) and a European Union HCM grant (ERB4001GT933623). We are grateful also to those who enthusiastically participated in the successful acquisition of logging-while-drilling data, a first for ODP.

Mike Underwood is kindly acknowledged for providing results on clay mineralogy of Hole 948C sediments, Jean Bahr, John Doveton, Dave Goldberg, Gerilynn R. Moline, and an anonymous reviewer for helpful comments, suggestions, and criticism.

REFERENCES

Alonso, B., Comas, M.C., Ercilla, G., and Palanques, A., 1996. Data report: textural and mineral composition of Cenozoic sedimentary facies off the western Iberian Peninsula, Sites 897, 898, 899, and 900. *In* Whitmarsh, R.B., Sawyer, D., et al., *Proc. ODP, Sci. Results*, 149: College Station, TX (Ocean Drilling Program), 741–751.

Biscaye, P.E., 1964. Distinction between kaolinite and chlorite in recent sediments by X-ray diffraction. *Am. Mineral.*, 49:1281–1289.

Burke, J.A., Curtis, M.R., and Cox, J.T., 1967. Computer processing of log data enables better production in Chaveroo field. *J. Pet. Technol.*, 19:889–895.

Doveton, J.H., and Cable, H.W., 1979. Fast matrix methods for the lithological interpretation of geophysical logs. *In* Gill D., Merriam, D.F. (Eds.) *Geomathematical and Petrophysical Studies in Sedimentology:* Oxford (Pergamon), 101–116.

Doveton, J.H., 1994. Geologic log analysis using computer methods. *AAPG Computer Appl. in Geol., 2:* Tulsa, OK (AAPG).

Fisher, A.T., and Underwood, M., 1995. Calibration of an X-ray diffraction method to determine relative mineral abundances in bulk powders using matrix singular value decomposition: a test from the Barbados accretionary complex. *In* Shipley, T.H., Ogawa, Y., Blum, P., et al., *Proc ODP, Init. Repts.*, 156: College Station, TX (Ocean Drilling Program), 29–37.

Giro, S., and Maldonado, A., 1985. Análisis granulométrico por métodos automáticos: tubo de sedimentación y Sedigraph. *Acta Geol. Hisp.*, 20:95–102.

International Centre For Diffraction Data, 1994. *Powder Diffraction Standards Files*. Newtown Square, PA.

Mascle, A., Moore, J.C., et al., 1988. *Proc ODP, Init. Repts.*, 110, College Station, TX (Ocean Drilling Program).

Moore, G.F., Zhao, Z., Shipley, T.H., Bangs, N., and Moore, J.C., 1995. Structural setting of the Leg 156 area, northern Barbados Ridge accretionary prism. *In* Shipley, T., Ogawa Y., Blum, P., et al., *Proc ODP, Init. Repts.*, 156: College Station, TX (Ocean Drilling Program), 13–27.

Moore, J.C., Mascle, A, Taylor, E., Andreieff, P, Alvarez, P., Barnes, R., Beck, C., Behrmann, J., Blanc, G., Brown, K., Clark, M., Dolan, J., Fisher, A., Gieskes, J., Hounslow, M., McLellan, P., Moran, K., Ogawa, Y., Sakai, T., Schoonmaker, J., Vrolijk, P., Wilkens, R., and Williams, C., 1988. Tectonics and hydrogeology of the northern Barbados Ridge: results from Ocean Drilling Program Leg 110. *Geol. Soc. Am. Bull*, 100:1578–1593.

Palanques, A., Plana, F., and Maldonado, A., 1990. Recent influence of man on the Ebro margin sedimentation system, northwestern Mediterranean Sea. *Mar. Geol.*, 95:247–263.

Rius, J., Plana, F., Palanques, A., 1989. A standardless X-ray diffraction method for the quantitative analysis of multiphase mixtures. *Appl. Crystallogr.*, 20:457–460.

Savre, W.C., 1963. Determination of a more accurate porosity and mineral composition in complex lithologies with the use of the sonic, neutron and density surveys. *J. Pet. Technol.* 15:945–959.

Schlumberger, 1982. *Natural Gamma Ray Spectrometry—Essentials of NGS interpretation:* Houston (Schlumberger).

Schlumberger, 1985. *Log Interpretation Charts:* New York (Schlumberger).

Schlumberger Educational Services, 1992. *Logging While Drilling:* Houston (Schlumberger).

Serra, O., 1986. Advanced interpretation of wireline logs: Houston (Schlumberger).

Shipboard Scientific Party, 1995. Explanatory Notes. *In* Shipley, T., Ogawa, Y., Blum, P., et al., *Proc ODP, Init. Repts.*, 156: College Station, TX (Ocean Drilling Program), 39–68.

Shipley, T., Ogawa, Y., Blum, P., et al., 1995. *Proc ODP, Init. Repts.*, 156: College Station, TX (Ocean Drilling Program).

Vatan, M., 1967. *Manuel de Sédimentologie:* Paris (Technip).

Date of initial receipt: 6 February 1996
Date of acceptance: 25 September 1996
Ms 156SR-028

Table 4. Comparison between averaged values of core sample analyses results and averaged values calculated by the inversion model.

Average values for the interval 420–570.5 mbsf at Site 948	Clay (%)	Smectite in clay (%)	Illite in clay (%)	Kaolinite + Chlorite in clay (%)	Kaolinite in clay (%)	Chlorite in clay (%)	$CaCO_3$ (wt%)
Core sample analyses (n = 28)	76.614	44.964	11.536	43.286	28.393	14.893	8.796
Inversion model	79.826*	40.637**	14.305**	45.046*	11.198**	33.882*	—

Notes: wt% = weight percent; * = n of 1003, ** = n of 1004. — = not computed in the model.